LM-02K037
May 13, 2002

Defect Structure and Evolution in Silicon Carbide Irradiated to 1 dpa-SiC at 1100°C

D.J. Senor, G.E. Youngblood, L.R. Greenwood, D.V. Archer,
D.L. Alexander, M.C. Chen, G.A. Newsome

NOTICE

Defect Structure and Evolution in Silicon Carbide Irradiated to 1 dpa-SiC at 1100°C

DJ Senor, GE Youngblood, LR Greenwood, DV Archer, DL Alexander

Pacific Northwest National Laboratory
P.O. Box 999, MSIN P8-10
Richland, WA 99352

MC Chen, GA Newsome

Lockheed Martin Corporation
P.O. Box 1072
Schenectady, NY 12301

Abstract

Transmission electron microscopy (TEM), swelling measurements, isochronal annealing, and thermal diffusivity testing were used to characterize the effects of radiation damage in SiC. Together, these techniques provided a comprehensive set of tools for observing and characterizing the structure and evolution of radiation-induced defects in SiC as a function of irradiation temperature and dose. In this study, two types of dense, crystalline, monolithic SiC were subjected to irradiation doses up to 1 dpa-SiC at a temperature of 1100°C, as well as post-irradiation annealing up to 1500°C. The microscopic defect structures observed by TEM were correlated to changes in the macroscopic dimensions, thermal diffusivity and thermal conductivity. The results demonstrated the value of using ultrapure β-SiC as an effective reference material to characterize the nature of expected radiation damage in other, more complex, SiC-based materials such as SiC/SiC composites.

PACS-1996 Codes

61.72.Ji Point defects and defect clusters
61.80.Hg Neutron radiation effects
66.70.+f Non-electronic thermal conduction and heat-pulse propagation
81.05.Je Ceramics and refractories

Keywords

Silicon carbide
Neutron radiation effects
Point defect structure and evolution
Irradiation-induced swelling
Transmission electron microscopy
Thermal diffusivity and conductivity

1. Introduction

Silicon carbide (SiC) possesses many desirable attributes for high-temperature applications in a neutron radiation environment. These include excellent dimensional and thermodynamic stability, low activation, high strength and high thermal conductivity. For these and other reasons, SiC-based materials currently are being considered for use in a variety of fusion energy systems as first wall or blanket structural materials. Monolithic SiC is a brittle ceramic, so structural applications likely will involve SiC fiber-reinforced composites. However, an understanding of the fundamental mechanisms for radiation damage in monolithic SiC is necessary to adequately predict the performance of SiC composites.

2. Experimental

2.1 Materials

The two types of monolithic SiC examined were chemical vapor deposited (CVD) SiC and Hexoloy SA, commercial products manufactured by Morton Advanced Materials and the Carborundum Corporation, respectively. The CVD SiC was fabricated by decomposing methyltrichlorosilane (MTS) gas onto a carbon substrate at 1350°C. The deposited material was extremely pure, with typical impurity concentrations of less than 5 wppm. The crystal structure was cubic, specifically the 3C polytype, commonly referred to as β-SiC. The grain size of the CVD SiC was between 5 and 10 μm in the plane parallel to the substrate, but the grains were elongated in the growth direction (perpendicular to the substrate). The material was typically free of microcracks and other large flaws, but atomic layer stacking faults were common. There was no porosity in the CVD SiC, and the material was essentially theoretically dense (approximately 3.21 g/cm^3).

The Hexoloy SA material was pressureless sintered from submicron SiC powder using boron (0.6 w/o) as a sintering aid in the form of B_4C. The material contained uniform micron-scale pores, and had a bulk density of approximately 98% theoretical (3.15 g/cm^3). The crystal structure was hexagonal, specifically the 6H polytype, commonly referred to as α-SiC. The microstructure of the material

consisted of equiaxed fine-grains of 4 to 6 μm diameter, with pores and B_4C precipitates typically found at grain triple points.

2.2 Irradiation conditions

The test materials were irradiated in multiple B-holes at the Advanced Test Reactor (ATR), a thermal reactor located at the Idaho National Environmental and Engineering Laboratory (INEEL). The samples were contained in two separate capsules that were irradiated for different lengths of time. Both capsules initially were irradiated from 20 May 1995 to 14 January 1996 for a total exposure of 4877 megawatt-days (185.0 effective full power days [EFPD] at 26.36 MW). One of the capsules was irradiated further, until 11 August 1996, for a total exposure of 9287 megawatt-days (358.3 EFPD at 25.92 MW). Post-irradiation dosimetry analysis was conducted on sections cut at different axial locations from the stainless steel capsule walls. The activation rates measured by gamma spectroscopy at each axial position together with the neutron energy spectrum and the appropriate activation cross-sections were used to determine the energy-dependent neutron flux. Using a detailed ATR power history, the fluence values for the test specimens were determined to range from 0.43-0.67 x 10^{25} n/m^2 (E>0.11 MeV) for the short-term capsule and 0.85-1.2 x 10^{25} n/m^2 (E>0.11 MeV) for the long-term capsule. Radiation damage calculations for SiC were made using threshold displacement energies of 35 eV for Si and 21 eV for C [1]. The dose received by the samples in the short-term capsule (referred to as the low-dose samples) ranged from 0.45 dpa-SiC to 0.70 dpa-SiC, while the samples in the long-term capsule (the high-dose samples) received between 0.89 dpa-SiC and 1.3 dpa-SiC.

Both the short-term and long-term capsules were designed to operate at approximately 1090°C, but they were not instrumented to allow verification of the irradiation temperature. However, isochronal annealing experiments on CVD SiC thermal expansion specimens revealed that the irradiation temperature was greater than 800°C (the temperature above which passive SiC temperature monitors cease to provide useful information) and less than 1200°C (the temperature beyond which void swelling effects would be observed). Also, the thermal diffusivity measured at lower temperatures following an

1100°C anneal increased by no more than a few percent over those data obtained before annealing at 1100°C. The minimal recovery in thermal diffusivity suggests that the irradiation temperature was only slightly lower than 1100°C, and most likely close to the design temperature of 1090°C. For simplicity, the irradiation temperature will be assumed to be 1100°C.

2.3 Test methods

Rectangular bars having nominal dimensions of 0.64 x 0.32 x 3.8 cm were measured to determine axial length changes caused by irradiation. The pre-irradiation measurements were made with a Sony Model DG2025N Digital Gaging Probe with a resolution of ±2.5 μm. The post-irradiation measurements were made using a Bausch & Lomb DR-25C optical gage with a resolution of ±0.25 μm. Cross-checks with calibrated standards eliminated the experimental bias introduced by using two different instruments for the pre- and post-irradiation measurements.

For the transmission electron microscope (TEM) examination, thermal diffusivity specimens with nominal dimensions of 0.95 cm diameter x 0.30 cm thick were cut into 100-150 μm thick sections perpendicular to the disk surfaces using a low-speed saw and a clean diamond blade. Sections of suitable size were cut into TEM disks using a diamond-tipped core drill. The disks were ground flat and dimpled using a rotating spherical grinding bit in fine diamond paste. After dimpling, the disks were ion polished with 5 keV Ar^+ ions on one side. Ion polishing continued until the disks were perforated in at least one location. Transmission electron microscopy was conducted using a JEOL 2010F microscope with a field-emission gun. The samples were examined primarily with bright-field imaging, but high-resolution images also were obtained at magnifications up to 1.5 x 10^6 X. Selected area diffraction patterns were produced to identify the crystal structure and orientation on representative samples.

Thermal diffusivity measurements were made via the laser flash method using two different systems. Measurements were made in static air from room temperature to 500°C on a system using a 50 J Nd:YAG laser as the heat source, and from 400°C to 1500°C in flowing Ar using a system with a 25 J ruby laser as the heat source. Both systems used an indium antimonide (InSb) infrared detector to observe the sample

back-surface temperature response. Neutral density filters were used in both systems at elevated temperatures to reduce thermal noise. In addition, divergent or diffusing quartz lenses were occasionally used to reduce and defocus the laser energy to minimize the sample front-surface temperature rise and reduce flashthrough. The data were reduced using the Koski method, with corrections for sample heat losses and finite laser pulse widths [2].

Isochronal annealing experiments were conducted on both thermal expansion and thermal diffusivity specimens. The thermal expansion specimens, having nominal rectangular dimensions of 0.51 x 0.19 x 3.8 cm, were annealed in an Anter Model 1161H(A1)D2-0 horizontal dual sample dilatometer system with absolute displacement transducers that allowed in-situ length measurements to be made after each isochronal anneal. The dilatometer furnace temperature initially was raised to 175°C and held for 30 min for a pre-test in-situ length measurement. Following this initial hold, the temperature was raised to 500°C at 10°C/min, where it was held for 120 min. The temperature was then decreased to 175°C at 10°C/min and held for 30 min for a post-anneal in-situ length measurement. This cycle was repeated a total of ten times, with each subsequent anneal temperature increasing by 100°C up to a final anneal at 1400°C. The anneal temperatures were taken as the average sample temperature during each 120-min hold, and the sample lengths were taken as the average lengths measured during the last 15 min of each 30-min hold at 175°C. Furnace temperature typically varied by less than ±5°C during the holds. Isochronal anneals on the thermal diffusivity specimens were conducted in the high-temperature diffusivity unit. The initial measurements were made in the as-irradiated condition from 400 to 1000°C, followed by a 60-min anneal at 1100°C. Thermal diffusivity was then measured on a decreasing temperature leg to 400°C. Subsequent tests followed similar procedures, with the anneal temperature increasing in 100°C steps to an ultimate anneal at 1500°C.

3. Results and discussion

3.1 Swelling measurements

Literature data show that at temperatures below 800°C, the swelling of SiC decreases approximately linearly with increasing temperature [3]. The swelling is caused by relaxation of the crystal lattice resulting from the presence of irradiation-induced point defects (interstitials and vacancies). As the irradiation temperature approaches 1000°C, two effects combine to reduce bulk swelling in SiC to almost zero. The mobility of the interstitial atoms increases, resulting in more vacancy-interstitial recombination. The increased mobility also causes the interstitials to form large, stable dislocation loops [4,5]. These structures are relatively coherent with the surrounding SiC matrix, resulting in little swelling. As the irradiation temperature approaches 1200°C, the vacancies become mobile and begin to coalesce into voids, although the onset of void swelling has not been well defined. Swelling in the void formation regime is strongly dose-dependent and non-linear with irradiation temperature [4].

There are relatively few swelling data in the literature for SiC irradiated between 1000°C and 1200°C. However, at temperatures below about 900°C, it generally has been observed that irradiation damage saturates at a fast fluence of 0.3-0.6 x 10^{25} n/m^2 [6]. The fast fluence achieved in this study was in this range, so defect accumulation in the samples may not have been saturated, particularly in the low-dose samples. Blackstone and Voice [7] noted a slow, linear increase in SiC swelling (unrelated to void swelling) as a function of dose at irradiation temperatures above 900°C following a rapid increase in swelling up to a pseudo-equilibrium near 0.3-0.6 x 10^{25} n/m^2. This phenomenon was attributed to interstitial defect clustering. A similar trend was observed by Price [8] at temperatures of 900°C and 1150°C. Yano, et al. [9] demonstrated that at temperatures below 650°C, swelling actually decreased as a function of increasing dose due to time-dependent agglomeration of interstitial point defects into dislocation loops. Finally, dose rate effects may affect the saturation dose in SiC. Temperature monitor calibration studies conducted by Palentine [6] demonstrated that the point defect concentration in thermal reactor temperature monitors was higher than in fast reactor temperature monitors at the same fast

fluence. Thus, it may follow that the saturation fluence in thermal reactors is somewhat higher than 0.3-0.6 x 10^{25} n/m^2, which was determined primarily from irradiation experiments in fast reactors.

Average length change data are presented in Table 1 for CVD SiC and Hexoloy SA. The data display a consistent trend of increased swelling with dose for both materials. This suggests a distinct dose dependence, with the swelling at the higher dose being a factor of 1.5 to 1.8 times that of the swelling at the lower dose. The dose dependence could be caused by either a higher saturation dose for point defects at 1100°C or void swelling.

The expected effects of void swelling in SiC are shown in Fig. 1 [4]. The linear swelling data from Table 1 are plotted in Fig. 1 for comparison with the Price data. The curves drawn through the Price data represent swelling for fluences from 5-8 x 10^{25} n/m^2 (E > 0.18 MeV in the Engineering Test Reactor [ETR]), which is roughly 5 to 10 times higher fluence than that received by the samples in the present study. The swelling data from the present study appear consistent with the Price data and seem to suggest the onset of void swelling, although the swelling data alone are not conclusive and may be merely a consequence of the fact that the swelling has not yet reached saturation. The swelling of Hexoloy SA is roughly 50% higher than that of CVD SiC. The higher swelling in Hexoloy SA presumably was due to the B sintering aid which promoted swelling by the formation of He within the α-SiC lattice via the $^{10}B(n,\alpha)^7Li$ reaction in the thermal spectrum of the ATR.

3.2 Transmission electron microscopy

To better understand the microstructural mechanisms behind the swelling behavior, several CVD SiC and Hexoloy SA samples were examined by transmission electron microscopy (TEM). One unirradiated and four irradiated CVD SiC thermal diffusivity specimens were prepared as TEM samples. Similarly, one unirradiated and two irradiated Hexoloy SA thermal diffusivity specimens were prepared for TEM examination. The irradiated CVD SiC specimens included one from each capsule, and one from each capsule that was subsequently subjected to isochronal annealing up to 1500°C during thermal diffusivity testing. The irradiated Hexoloy SA specimens included one from each capsule. The TEM samples, their

irradiation conditions and post-irradiation thermal treatments are listed in Table 2 along with data for dislocation loop average diameter and density.

Fig. 2a depicts the unirradiated CVD SiC material and clearly shows the columnar grain structure in the <111> CVD growth direction (parallel to the plane of the image) and the faulted microstructure. The grain boundaries were clean and free of porosity or precipitates. The low-dose as-irradiated CVD SiC specimen is shown in Fig. 2b. The microstructure contains stacking faults with a density and spacing similar to that observed in unirradiated CVD SiC, but there is also a significant quantity of defects not present in the unirradiated material. The defects, appearing as either black spots or partially resolved rings, are most likely interstitial dislocation loops. Price [4] determined that defects similar to these in β-SiC were Frank dislocation loops lying on {111} planes. The defects in the low-dose as-irradiated sample range in diameter from about 1.5 nm to about 6.7 nm, with an average diameter of 3.4 nm and an areal density in the plane of the micrograph of about 4.7×10^{-3} loops/nm^2. Fig. 2c shows representative images of the high-dose as-irradiated CVD SiC specimen. The microstructure is very similar to that observed in the low-dose specimen shown in Fig. 2b. The dislocation loops range in diameter from about 1.7 nm to about 8.3 nm, with an average of about 3.9 nm and a density of approximately 2.5×10^{-3} loops/nm^2. Thus, the size of the dislocation loops appears to be slightly larger and the loop density slightly lower for the high-dose (0.90 dpa-SiC) specimen compared to the low-dose (0.49 dpa-SiC) specimen. The measured defect sizes and densities are comparable to values previously reported in the literature for irradiated β-SiC [4,5,9,10,11]. These data are summarized in Fig. 3, which depicts average loop diameter as a function of irradiation temperature and fast fluence. From the data, it appears that loop diameters tend to be larger at high fluence and low temperature. Below a fluence of 10^{25} n/m^2 and above a temperature of 800°C, the dependence of loop diameter on fluence and irradiation temperature appears to be less dramatic. These trends are somewhat counter-intuitive and in contrast to a phenomenological model of swelling in irradiated SiC developed by Huang and Ghoniem [12]. Their model, strictly valid only to 1000°C, predicts an increase in the average loop size with increasing temperature, which is consistent with a decrease in swelling with increasing temperature if interstitial defects are primarily responsible for

swelling in this temperature regime. Further, their model predicts loop sizes for saturated swelling conditions, and does not consider fluence dependence that may exist at higher irradiation temperatures. However, if the Huang and Ghoniem model is applied at 1100°C, it predicts average loop diameters of 18.2 nm. This is approximately a factor of five higher than the data obtained in the present study for CVD SiC. The discrepancy may be explained by the fact that their model was based on experimental data extending only to 1000°C and/or by the fact that the swelling of the CVD SiC samples in the present study may not have reached saturation at a dose of approximately 0.9 dpa-SiC.

Fig. 4a shows a representative image of the low-dose CVD SiC specimen annealed for 60 minutes at 1500°C. In general, its appearance is very similar to the two as-irradiated specimens. The dislocation loops range in diameter from 1.9 to 8.4 nm, with an average diameter of 4.2 nm and a density of 1.4×10^{-3} loops/nm^2. The loop diameter is 24% larger than the low-dose as-irradiated sample, and the corresponding density is about 70% lower. This trend is consistent with previous experimental data in which post-irradiation anneals at temperatures above 1400°C produced significant increases in loop diameter with corresponding decreases in loop density [9,10,13,14]. In these studies, the irradiations all were conducted at temperatures at or below 650°C. More significant loop growth appears to occur during annealing of specimens irradiated at lower temperatures. This observation suggests that there are more small, unstable interstitial clusters after irradiation at low temperatures, while at high temperatures virtually all of the interstitials are bound in more stable dislocation loops, resulting in less loop growth upon annealing.

Fig. 4b is a higher magnification image of the annealed low-dose sample showing a significant number of small voids. The voids were identified by making consecutive over- and under-focused images, and observing the contrast change of the suspected voids. The voids were small (about 3 nm in diameter), and their distribution did not appear to be uniform or random. They were not found along grain boundaries, but typically were lined up along certain crystallographic planes parallel to stacking faults. Price [4] noted similar voids after irradiation at temperatures in excess of 1250°C. He observed that a band 10 to 50 nm wide on either side of grain boundaries tended to be free of voids, and that the

voids within the grains showed a preference for aligning parallel to the {111} planes along stacking faults. The voids in Fig. 4b are likely the result of vacancy diffusion and coalescence during the post-irradiation anneals at temperatures above 1200°C, because voids were not observed in significant numbers in the unirradiated or as-irradiated specimens. Thus, an irradiation temperature of 1100°C does not appear to lie within the void swelling regime, even though the swelling behavior shown in Fig. 1 is suggestive of this mechanism.

Fig. 4c shows a high-magnification TEM image obtained from the high-dose CVD SiC specimen annealed for 60 minutes at 1500°C. The appearance of this specimen is similar to the annealed low-dose sample. The dislocation loops in the annealed high-dose specimen are significantly larger than in the other three irradiated samples, with diameters ranging from 1.8 nm to 15 nm, an average diameter of 7.2 nm and a density of 1.3×10^{-3} loops/nm^2. The average loop diameter is 85% higher than the high-dose as-irradiated sample, and the loop density is approximately 48% lower. Typical void size is about 5 nm in diameter, although some are significantly larger. Thus, not only are the dislocation loops larger in this specimen relative to the low-dose annealed sample, but the voids appear to be larger as well, suggesting a higher concentration of vacancies were available for void coalescence and growth during the post-irradiation anneals.

A representative TEM image of the unirradiated Hexoloy SA specimen is shown in Fig. 5a. The α-SiC microstructure is clean, with far fewer stacking faults compared to the unirradiated β-SiC shown in Fig. 2a. This undoubtedly is due to the higher processing temperature of the α-SiC. A few precipitates are visible in Fig. 5a, mostly along grain boundaries and at grain triple points. They typically are a few hundred nanometers in diameter, and are probably B_4C. A representative TEM micrograph of the low-dose irradiated Hexoloy SA specimen is shown in Fig. 5b. Two types of irradiation-induced defects were observed in this specimen. In Fig. 5b, a grain triple point is shown with a significant concentration of dislocation loops within the grains and a large number of bubbles along the grain boundaries. The bubbles likely were caused by the formation of He via the $^{10}B(n,\alpha)^7Li$ reaction. Although bubbles were

not observed on all the grain boundaries, they were observed on a significant fraction of them throughout the TEM sample. The bubbles were densely and uniformly distributed across the entire grain surface when the grain boundaries were tilted with respect to the electron beam axis. The bubbles did not appear to be circular, but generally were flattened in shape, with the long axis parallel to the grain boundary. The bubbles ranged in size from about 5 nm to over 60 nm on the long axis. The bubbles observed in this sample are similar to (although larger than) those reported in the literature on B-containing SiC specimens irradiated at lower temperatures with subsequent post-irradiation anneals at temperatures above 1200°C [15,16]. The dislocation loops in this sample have much the same appearance as those observed in the CVD SiC specimens, but they seem to be slightly larger in Hexoloy SA at the same fluence. For example, the dislocation loops in Fig. 5b range in size from 1.4 nm to 9.3 nm, with an average diameter of 4.6 nm and a density of 3.6×10^{-3} loops/nm^2. The average loop diameter is approximately 35% larger than the low-dose as-irradiated CVD SiC specimen, and the density is approximately 23% lower.

Fig. 5c shows an image of the high-dose irradiated Hexoloy SA specimen. In general, its appearance is similar to the low-dose Hexoloy SA sample. In both irradiated samples, regions were observed in which the bubbles aligned along stacking faults rather than grain boundaries. Fig. 5c shows such a region, with bubbles along one stacking fault but not on two other nearby faults. The dislocation loops in the high-dose sample ranged in size from 1.9 nm to 9.3 nm, with an average diameter of 4.4 nm and a density of 5.2×10^{-3} loops/nm^2. The average loop diameter and density are higher than those measured on the high-dose as-irradiated CVD SiC sample, but very similar to those measured for the low-dose Hexoloy SA specimen. The bubbles have essentially the same shape as those observed in the low-dose Hexoloy SA sample, and their size range is approximately the same. Calculations demonstrate that all the B in Hexoloy SA would likely be burned up in the ATR neutron spectrum in approximately 100 EFPD. Both the low- and high-dose Hexoloy SA samples were irradiated to much higher exposures (185 and 358 EFPD, respectively). Therefore, both the low- and high-dose Hexoloy SA samples should have the same amount of swelling due to He bubbles resulting from B depletion, and the observed difference in bulk swelling between the low- and high-dose samples must be due to point defect swelling alone. This

observation is supported by the fact that the difference in swelling between the low- and high-dose samples is the same for both CVD SiC and Hexoloy SA.

3.3 Thermal diffusivity measurements

Fig. 6 provides a comparison of the measured thermal diffusivity for nine irradiated CVD SiC samples and one unirradiated CVD SiC sample. The thermal diffusivity of each specimen was measured before and after irradiation, but for the purposes of comparison the diffusivity of the unirradiated sample in Fig. 6 may be taken as representative of this batch of Morton CVD SiC. Note that the degradation in thermal diffusivity is larger for the high-dose samples (indicated by the open symbols and dashed lines in Fig. 6). The dose dependence is most noticeable below about 500°C, and is clearly evident in the room temperature diffusivity data of Fig. 7. The difference in room temperature diffusivity between the low-dose (about 0.48 dpa-SiC) and high-dose (about 0.91 dpa-SiC) samples is significant, with the low-dose samples averaging about 0.45 cm^2/s and the high-dose samples averaging about 0.32 cm^2/s. Based on the thermal diffusivity data, the irradiation damage in CVD SiC does not appear to be saturated up to a dose of approximately 0.9 dpa-SiC. This observation is consistent with the dose dependence observed in the CVD SiC swelling data described above. It appears that the saturation dose of irradiation-induced point defects increases at high irradiation temperatures, as noted by Blackstone and Voice [7] and Price [8].

Fig. 8 provides a comparison of the measured thermal diffusivity for eight irradiated and two unirradiated Hexoloy SA samples. The high-dose samples display greater diffusivity degradation in a manner similar to that shown in Fig. 6 for CVD SiC. The difference in room temperature diffusivity between the low-dose (about 0.47 dpa-SiC) and high-dose (about 0.93 dpa-SiC) samples is significant, with the low-dose samples averaging about 0.21 cm^2/s and the high-dose samples averaging about 0.17 cm^2/s. The relative diffusivity degradation of the CVD SiC and Hexoloy SA appears to be similar, suggesting that the presence of the bubbles in irradiated Hexoloy SA does not significantly degrade the diffusivity in comparison to the distributed point defects (i.e. vacancies).

3.4 Isochronal annealing

Four irradiated CVD SiC thermal expansion specimens and two irradiated thermal diffusivity specimens were selected for isochronal annealing. The thermal expansion specimens included two 0.53 dpa-SiC samples and two 1.1 dpa-SiC samples. The isochronal annealing data for the four thermal expansion specimens are shown in Fig. 9, with the high-dose samples represented by open symbols. All the curves appear similar, independent of dose. No length decrease associated with point defect annealing is observed, as expected for the high (1100°C) irradiation temperature. However, the length increases above 1000°C, and particularly above 1300°C, appear to be a real effect. This behavior is reminiscent of length increases observed by Suzuki, et al. [17] in irradiated SiC specimens that contained small He bubbles. In these materials, the irradiation-induced vacancies became mobile at annealing temperatures of 1300°C and were driven to coalesce with the He bubbles due to a mismatch between bubble stored energy and bubble surface energy. An analogous process of vacancy migration and void coalescence appears to have taken place in the irradiated CVD SiC samples after the annealing temperature exceeded 1200°C. Small (3 to 5 nm) voids were observed in TEM micrographs along stacking faults in irradiated CVD SiC samples annealed at 1500°C, as described previously. The production of these voids must have been sufficient to increase the length of the thermal expansion specimens by the amounts shown in Fig. 9.

The thermal diffusivity specimens selected for isochronal annealing included one 0.48 dpa-SiC sample and one 0.91 dpa-SiC sample. Previous studies have demonstrated that the swelling caused by irradiation-induced interstitial point defects at irradiation temperatures less than 800°C can be completely eliminated by annealing to about 1300°C [17]. Under these circumstances, the diffusivity would be expected to fully recover as well, because the irradiation-induced phonon scattering sites would be completely eliminated. The thermal diffusivity data obtained during the isochronal annealing experiments on the low-dose and high-dose samples are shown in Fig. 10. Thermal diffusivity improved after each anneal, including the 1400 and 1500°C anneals. Below 1300°C, the cause of the diffusivity recovery most likely is vacancy-interstitial recombination or interstitial dislocation loop growth. After the 1300°C

anneal, all available interstitial atoms should have either recombined with vacancies or contributed to the growth of stable dislocation loops. Further recovery in thermal diffusivity beyond this temperature suggests some other mechanism is responsible for eliminating phonon scattering sites. The explanation for this behavior is diffusion of isolated vacancies resulting in coalescence in small voids such as those observed by TEM examination of the post-irradiation annealed CVD SiC samples. As expected, an increase in dislocation loop diameter and a decrease in loop concentration also was measured in the annealed specimens. Furthermore, the residual diffusivity degradation in the higher dose sample is greater than in the lower dose sample, suggesting the defect structures in the higher dose specimen is more stable. This observation is consistent with the larger dislocation loop size in the high-dose TEM specimen.

3.5 Point defect concentration calculations

To aid in the understanding of irradiation-induced defect structure and thermal diffusivity degradation mechanisms, point defect concentrations were estimated from the CVD SiC thermal diffusivity data. One way to express lattice thermal conductivity (k) is

$$k = \frac{1}{3} c_v v l \rho, \tag{1}$$

where c_v is the specific heat at constant volume, v is the phonon velocity, l is the phonon mean free path, and ρ is the density of the material [18]. Thermal conductivity also may be expressed as

$$k = \alpha c_p \rho \tag{2}$$

where α is the thermal diffusivity of the material and c_p is the specific heat at constant pressure. By comparing Eq. (1) with Eq. (2), it is apparent that thermal diffusivity may be expressed as

$$\alpha = \frac{1}{3} v l, \tag{3}$$

if one makes the assumption that c_v is approximately equal to c_p (generally valid to within 10% up to the melting point of the material [19]). Phonon velocity can be estimated from the speed at which vibrations propagate through an elastic material,

$$v = \sqrt{\frac{E}{\rho}}, \tag{4}$$

where E is the Young's modulus of the material [20]. For SiC, Eq. (4) yields a value of 1.1 x 10^5 cm/s, which is approximately constant as a function of temperature. Therefore, the temperature dependence of thermal diffusivity will be dominated by the temperature dependence of the phonon mean free path.

The phonon mean free path can be subdivided into contributions from various sources by inverting and expanding Eq. (3)

$$\frac{1}{\alpha} = \frac{3}{v}\sum_n \frac{1}{l_n} = \frac{3}{v}\left(\frac{1}{l_o} + \frac{1}{l_i} + \frac{1}{l_p}\right), \tag{5}$$

where the subscripts o, i, and p represent phonon mean free paths associated with intrinsic defects, irradiation-induced defects, and phonon-phonon interactions, respectively. If the concentration of intrinsic and irradiation-induced defects is assumed constant as a function of test temperature (a valid assumption below the irradiation temperature), then the temperature dependence of thermal diffusivity will be dominated by the temperature dependence of the mean free path associated with phonon-phonon interactions.

Above $T_o = \Theta_D/3$ (approximately 280K for SiC), the temperature dependence of l_p can be described by

$$l_p = \frac{b}{(T - T_o)}, \tag{6}$$

where b is a constant [18]. Substituting Eq. (6) into Eq. (5),

$$\frac{1}{\alpha} = \frac{3}{v}\left(\frac{1}{l_o} + \frac{1}{l_i} - \frac{T_o}{b} + \frac{T}{b}\right) = A + BT, \tag{7}$$

where

$$A = \frac{3}{v}\left(\frac{1}{l_o} + \frac{1}{l_i} - \frac{T_o}{b}\right), \tag{8}$$

and

$$B = \frac{3}{vb}. \tag{9}$$

The distribution of intrinsic and irradiation-induced point defects is assumed to be uniform. The spacing of these uniformly distributed defects is estimated by calculating the linear dimension (l_d) of a cubic volume surrounding each defect,

$$\frac{1}{l_d} = \frac{1}{l_o} + \frac{1}{l_i} = \left(\frac{a_o^3}{Nx}\right)^{-\frac{1}{3}}, \tag{10}$$

where a_o is the lattice parameter for β-SiC (0.436 nm), N is the number of atoms in the unit cell defined by a_o (8), and x is the fractional concentration of point defects (intrinsic plus irradiation-induced). A linear fit to reciprocal diffusivity data yields values for A and B from Eq. (7), and b can be determined from Eq. (9). The defect inverse mean free path then can be calculated from Eq. (8),

$$\frac{1}{l_d} = \frac{1}{l_o} + \frac{1}{l_i} = \frac{Av}{3} + \frac{T_o}{b}, \tag{11}$$

and the defect concentration can be calculated by solving for x in Eq. (10),

$$x = \frac{a_o^3}{N}\left(\frac{1}{l_d}\right)^3. \tag{12}$$

Using this approach, defect concentrations were calculated for the unirradiated and irradiated CVD SiC samples. Fig. 11 shows the reciprocal diffusivity data for the ten samples shown in Fig. 6, illustrating their linearity and agreement with the temperature dependence of Eq. (7). Because a minor amount of defect annealing was observed after the thermal diffusivity tests at 1100°C, only data taken prior to the 1100°C measurements are included in Fig. 11. The calculated pre- and post-irradiation defect mean free paths (l_d) and defect concentrations (x) are given in Table 3 for the CVD SiC specimens, along with A, B, and the correlation coefficients for the linear fits shown in Fig. 11. Similar data are provided in Table 4 for the two CVD SiC thermal diffusivity specimens subjected to post-irradiation isochronal anneals.

The A term in Eq. (7) yields information related to the concentration and distribution of defects. The calculated defect mean free paths and corresponding defect concentrations are very consistent for each of

the three conditions (i.e. unirradiated, irradiated, and irradiated/annealed). Further, the calculated defect mean free paths for the unirradiated specimens are the same order of magnitude as the stacking fault spacing in unirradiated CVD SiC. This suggests that the thermal diffusivity in the unirradiated condition is limited by phonon scattering on stacking faults. Note also the low concentration of defects in the unirradiated condition (<1 appm). These values are consistent with data quoted by the manufacturer [21] and neutron activation analysis data obtained on CVD SiC material from this batch, and they illustrate why CVD SiC makes an ideal irradiation damage monitor. The intrinsic concentration of point defects is very low, thereby allowing the presence of the irradiation-induced point defects to be clearly inferred.

The B term in Eq. (7) provides some insight into the nature of the defects. Note that the average B value of the two groups of irradiated specimens is approximately the same, and distinctly different from the B values of the unirradiated specimens. If the dominant phonon scattering mechanism in the unirradiated samples is the stacking faults, then the difference in B values between the unirradiated and irradiated specimens suggests that the dominant phonon scattering mechanism in the irradiated specimens is different. These observations are consistent with the calculated increase in defect concentrations, and suggest that irradiation-induced point defects (i.e. vacancies) represent the dominant phonon scattering mechanism in the irradiated samples.

Fig. 12 illustrates the relationship between defect mean free path, defect concentration and irradiation dose. Clearly, the concentration of point defects in the higher dose samples is greater than in the lower dose samples. Assuming that the irradiation temperatures were comparable for both capsules, these results indicate that irradiation damage at 1100°C does not saturate quickly like it does at lower temperatures. Indeed, it cannot be inferred from the data in Table 3 and Fig. 12 whether the point defect concentration continues to increase with dose indefinitely or if it eventually equilibrates at a dose somewhere above 0.9 dpa-SiC. However, even if the swelling continues at the same rate through 10 dpa-SiC, the total accumulated linear swelling will be only about 1%.

Point defect concentrations were calculated from the thermal diffusivity isochronal annealing data shown in Fig. 10. The results are shown in Fig. 13. There is some scatter in the calculated point defect

concentrations, but in general, they tend to decrease rapidly after the 1100°C anneal. The reduction in point defect concentration between 1100°C and 1300°C is the result of vacancy-interstitial recombination and/or interstitial dislocation loop growth. The more gradual reduction in point defect concentration above 1300°C likely is due to the elimination of isolated vacancies by the formation of voids. For both samples, as shown in Table 4, the defect concentrations calculated after the last anneal are still higher than before irradiation, suggesting the presence of remaining isolated vacancies. This is consistent with the fact that some diffusivity degradation remained in both irradiated samples after anneals at 1500°C.

3.6 Thermal conductivity calculations

Thermal diffusivity and room temperature density data were combined with calculated specific heat values to produce thermal conductivity values for each CVD SiC sample. The room temperature density data were corrected at high temperature using thermal expansion data. The specific heat values were calculated using a modified Debye theory approach that takes into consideration harmonic and anharmonic lattice vibrations, lattice dilation and electronic contributions to specific heat. The thermal conductivity trends mirror those of thermal diffusivity. Fig. 14 shows the ratio of unirradiated-to-irradiated thermal conductivity as a function of irradiation and test temperature for β-SiC from a variety of sources [22,23,24,25]. The data in Fig. 14 are useful to the fusion reactor and composite material designer because they define the physical limit to improvement of radiation damage tolerance in other SiC-based materials (e.g. SiC/SiC composites). The present data are reasonably consistent with the previous data, although there appears to be some fluence dependence above about 1000°C (i.e. less degradation at lower fluence for the same irradiation temperature).

4. Conclusions

The accumulation of irradiation-induced point defects in SiC-based materials irradiated near 1100°C is not saturated up to a dose of at least 0.9 dpa-SiC. The thermal diffusivity data correlate well with the linear swelling data in this regard. Both sources of data indicate that point defect concentrations increase

approximately linearly with dose in this temperature regime. The results of this study also indicate that void swelling in SiC is not observed at an irradiation temperature of 1100°C. These observations are supported by transmission electron microscopy of irradiated materials. It is not clear whether the accumulation of point defects continues to increase indefinitely at 1100°C or whether the defect concentration eventually saturates. This issue presents some concern with regard to dimensional stability and thermal performance for SiC-based materials irradiated to doses beyond 1 dpa-SiC at this temperature. Clearly, higher dose irradiation studies are warranted to determine the dose at which (or if) the point defect concentration equilibrates as a function of irradiation temperature.

Hexoloy SA swelling consistently exceeded that of CVD SiC. The excess swelling in Hexoloy SA was caused by helium bubbles on the grain boundaries resulting from thermal neutron (n,γ) reactions with ^{10}B (added to Hexoloy SA as a sintering aid). Interestingly, Hexoloy SA samples irradiated in previous fast reactor experiments did not exhibit greater swelling than other SiC-based materials, suggesting that He bubbles were either absent or negligible in quantity. Presumably, this was due to the absence of a significant thermal neutron flux in the fast reactors, resulting in negligible He production from the B sintering aid. With the exception of swelling caused by the He production, it appears that Hexoloy SA behaves very similarly to CVD SiC after irradiation to about 1 dpa-SiC at 1100°C.

Chemical vapor deposited SiC is particularly valuable as a reference material in the study of radiation damage. Because of its high purity and low intrinsic defect concentration, CVD SiC makes an excellent radiation damage monitor. Thermal diffusivity measurements on CVD SiC provide a simple method for determining defect concentrations, and isochronal annealing experiments (in conjunction with diffusivity and/or thermal expansion measurements) provide information on defect structure and stability. Further, the linearity of the inverse diffusivity data with temperature suggest that low-temperature measurements (quicker and less expensive than a combination of low- and high-temperature measurements) are sufficient to characterize the magnitude of radiation damage in SiC. Comparisons between other SiC-based materials and CVD SiC yields insight into the dominant damage mechanisms in those materials.

Finally, the behavior of CVD SiC defines the physical limit to improvement of radiation damage tolerance in other SiC-based materials such as SiC/SiC composites.

Acknowledgements

The Pacific Northwest National Laboratory is operated by Battelle for the U.S. Department of Energy. The authors express their appreciation to VY Guertsman and JS Vetrano for TEM sample preparation and examination.

References

[1] R. Devanathan and W.J. Weber, J. Nucl. Mater. 278 (2000) 258.

[2] J.A. Koski, in: J.V. Sengers, Ed., Proceedings of the 8th Symposium on Thermophysical Properties (The American Society of Mechanical Engineers, New York, 1981) pp. 94-103.

[3] R.J. Price. Nucl. Tech. 16 (1972) 536.

[4] R.J. Price, J. Nucl. Mater. 48 (1973) 47.

[5] T. Yano, T. Suzuki, T. Maruyama and T. Iseki. J. Nucl. Mater. 155-157 (1988) 311.

[6] J.E. Palentine. J. Nucl. Mater. 61 (1976) 243.

[7] R. Blackstone and E.H. Voice. J. Nucl. Mater. 39 (1971) 319.

[8] R.J. Price, Nucl. Tech. 35 (1977) 320.

[9] T. Yano, H. Miyazaki, M. Akiyoshi and T. Iseki. J. Nucl. Mater. 253 (1998) 78.

[10] T. Suzuki, T. Maruyama, T. Iseki, T. Mori and M. Ito. J. Nucl. Mater. 149 (1987) 334.

[11] T. Iseki, T. Maruyama, T. Yano, T. Suzuki and T. Mori. J. Nucl. Mater. 170 (1990) 95.

[12] H. Huang and N. Ghoniem. J. Nucl. Mater. 250 (1997) 192.

[13] R. Stevens. Phil. Mag. 25 (1972) 523.

[14] S.D. Harrison and J.C. Corelli. J. Nucl. Mater. 99 (1981) 203.

[15] T. Suzuki, T. Iseki, T. Mori and J.H. Evans. J. Nucl. Mater. 170 (1990) 113.

[16] K. Sasaki, T. Yano, T. Maruyama and T. Iseki. J. Nucl. Mater. 179-181 (1991) 407.

[17] T. Suzuki, T. Yano, T. Mori, H. Miyazaki and T. Iseki. Fusion Tech. 27 (1995) 314.

[18] H.M. Rosenberg. *Low Temperature Solid State Physics*. Oxford University Press, London (1963).

[19] A. Cezairliyan. *Specific Heat of Solids*. Hemisphere Publishing, New York (1988).

[20] H. Kolsky. *Stress Waves in Solids*. Dover Publications, New York (1963).

[21] Morton Advanced Materials. Technical Publication 107, Morton Advanced Materials (1996).

[22] D.J. Senor, G.E. Youngblood, C.A. Moore, D.J. Trimble, G.A. Newsome and J.J. Woods. Fusion Tech. 30 (1996) 943.

[23] R.P. Thorne, V.C. Howard and B. Hope. Proc. Brit. Ceram. Soc. 7 (1967) 449.

[24] R.J. Price. J. Nucl. Mater. 46 (1972) 268.

[25] M. Rohde. J. Nucl. Mater. 182 (1991) 87.

Figure Captions

Fig. 1. Comparison of flexure specimen linear swelling data to void swelling data

Fig. 2. TEM images of CVD SiC in the a) unirradiated, b) low-dose irradiated (0.49 dpa-SiC) and c) high-dose irradiated (0.90 dpa-SiC) conditions

Fig. 3. Average dislocation loop diameter in β-SiC as functions of a) irradiation temperature (numbers indicate fast neutron fluence in 10^{25} n/m^2) and b) fast neutron fluence (numbers indicate irradiation temperature in °C)

Fig. 4. TEM images of irradiated CVD SiC subjected to a post-irradiated anneal at 1500°C a) at moderate magnification showing the general appearance of the low-dose specimen (0.48 dpa-SiC), b) at higher magnification showing voids in the low-dose specimen, and c) showing the voids in the high-dose specimen (0.91 dpa-SiC)

Fig. 5. TEM images of Hexoloy SA in the a) unirradiated, b) low-dose irradiated (0.47 dpa-SiC) and c) high-dose irradiated (0.94 dpa-SiC) conditions

Fig. 6. Thermal diffusivity of CVD SiC in the unirradiated (open symbols with solid lines), low-dose irradiated (closed symbols with solid lines) and high-dose irradiated (open symbols with dashed lines) conditions

Fig. 7. Room temperature thermal diffusivity of CVD SiC as a function of irradiation dose

Fig. 8. Thermal diffusivity of Hexoloy SA in the unirradiated (open symbols with solid lines), low-dose irradiated (closed symbols with solid lines) and high-dose irradiated (open symbols with dashed lines) conditions

Fig. 9. Isochronal annealing data for irradiated CVD SiC thermal expansion specimens (high-dose samples indicated by open symbols)

Fig. 10. Thermal diffusivity of CVD SiC before irradiation, after irradiation to a) 0.48 dpa-SiC and b) 0.91 dpa-SiC, and after post-irradiation isochronal annealing

Fig. 11. Reciprocal thermal diffusivity of unirradiated and irradiated CVD SiC showing the linear fits used to calculate defect concentrations

Fig. 12. Defect mean free path and point defect concentrations for CVD SiC calculated from reciprocal thermal diffusivity data as a function of irradiation dose

Fig. 13. Point defect concentrations in CVD SiC calculated from reciprocal thermal diffusivity data as a function of post-irradiation anneal temperature

Fig. 14. Ratio of irradiated to unirradiated thermal conductivity of β-SiC measured at the irradiation temperature

Fig. 1.

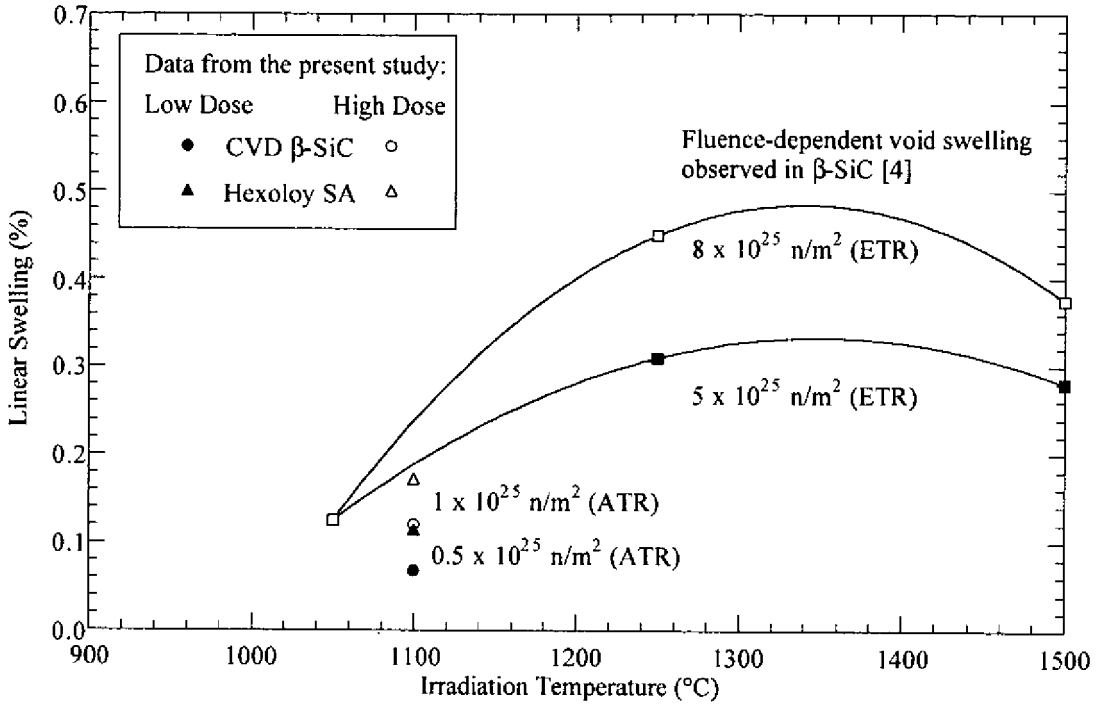
Data from the present study:
Low Dose
High Dose
CVD β-SiC
Hexoloy SA
Fluence-dependent void swelling observed in β-SiC [4]
8 x 10^25 n/m^2 (ETR)
5 x 10^25 n/m^2 (ETR)
1 x 10^25 n/m^2 (ATR)
0.5 x 10^25 n/m^2 (ATR)
Linear Swelling (%)
Irradiation Temperature (°C)
0.0
0.1
0.2
0.3
0.4
0.5
0.6
0.7
900
1000
1100
1200
1300
1400
1500

Fig. 2.

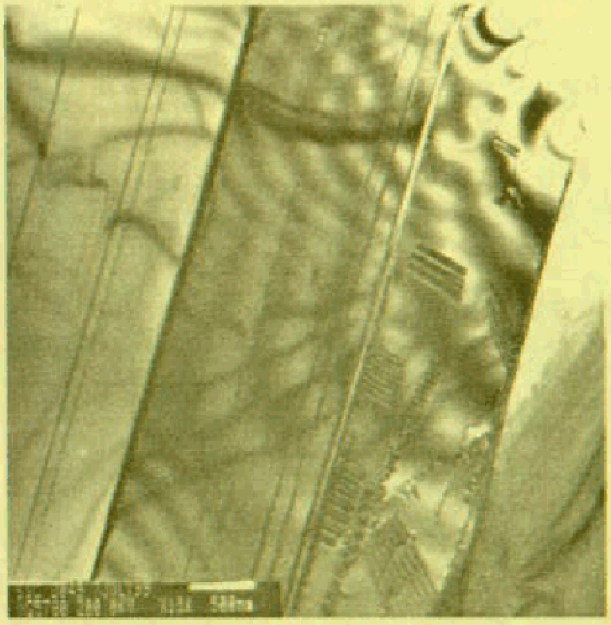

(a)

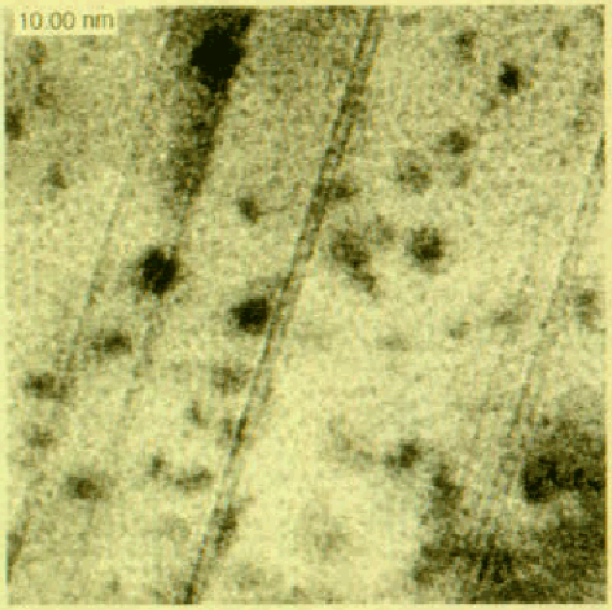

(b)

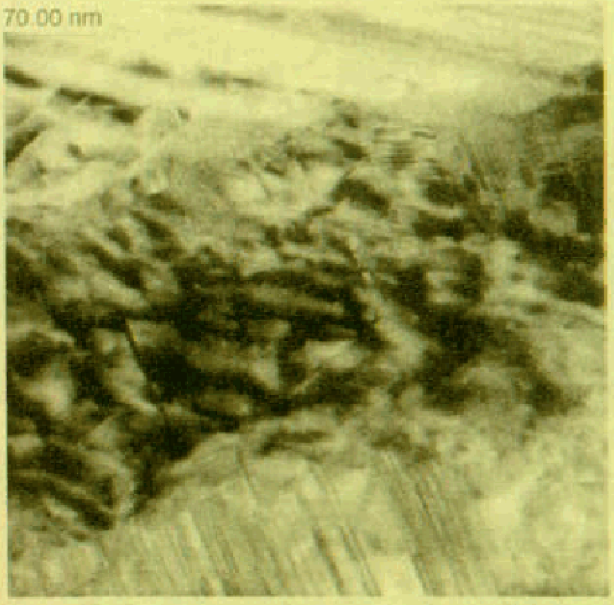

(c)

Fig. 3.

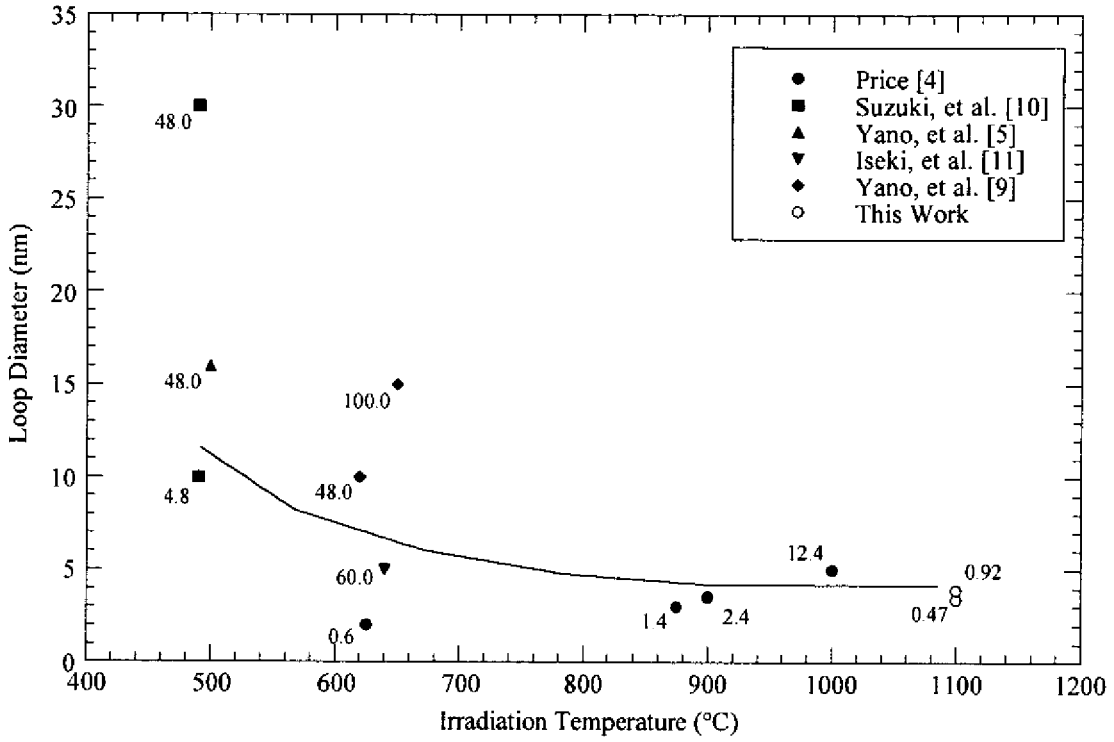
Price [4]
Suzuki, et al. [10]
Yano, et al. [5]
Iseki, et al. [11]
Yano, et al. [9]
This Work
Loop Diameter (nm)
Irradiation Temperature (°C)
48.0
48.0
100.0
4.8
48.0
60.0
0.6
12.4
0.92
1.4
2.4
0.47
0
5
10
15
20
25
30
35
400
500
600
700
800
900
1000
1100
1200

(a)

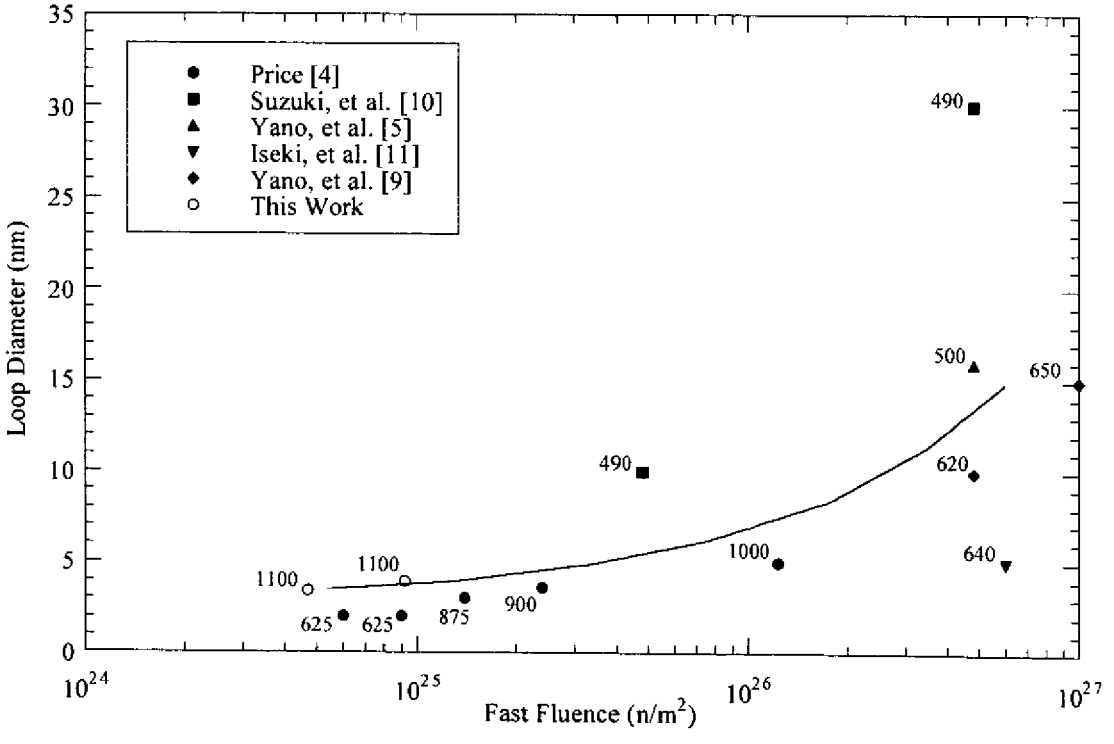
Price [4]
Suzuki, et al. [10]
Yano, et al. [5]
Iseki, et al. [11]
Yano, et al. [9]
This Work
Loop Diameter (nm)
Fast Fluence (n/m^2)
490
500
650
490
620
1000
640
1100
1100
625
625
875
900
0
5
10
15
20
25
30
35
10^{24}
10^{25}
10^{26}
10^{27}

(b)

Fig. 4.

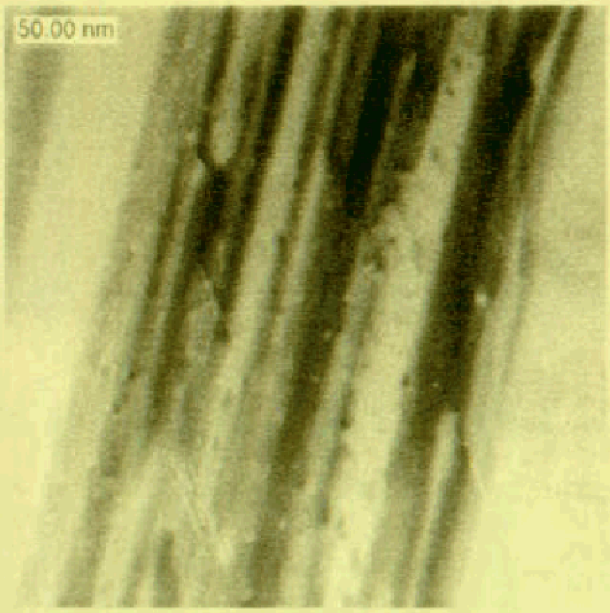

(a)

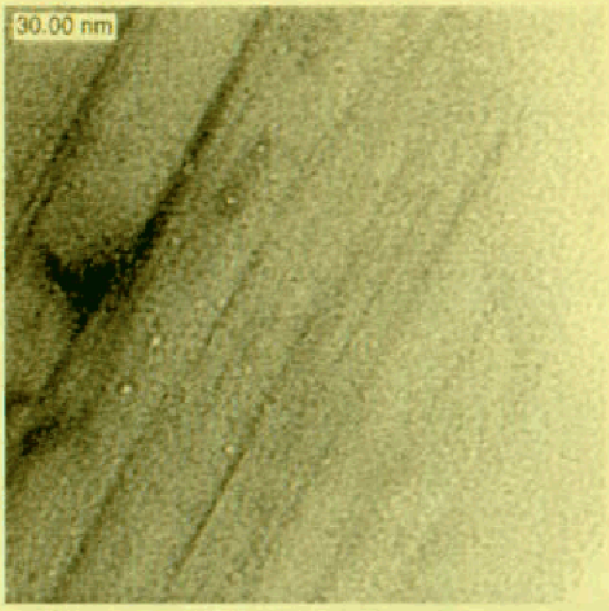

(b)

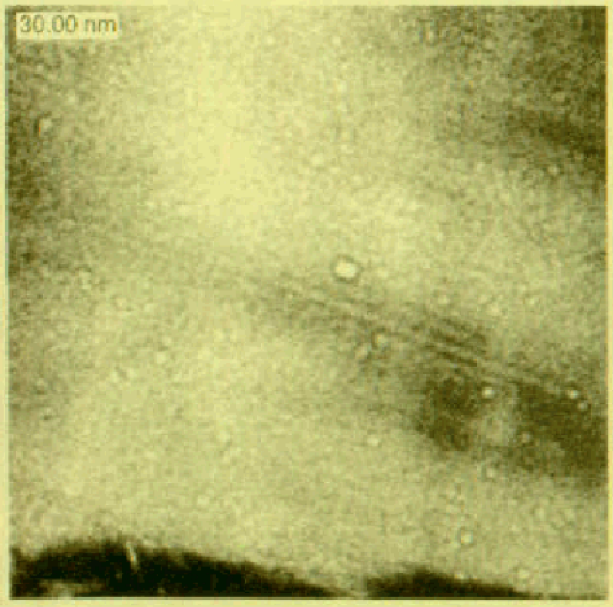

(c)

Fig. 5.

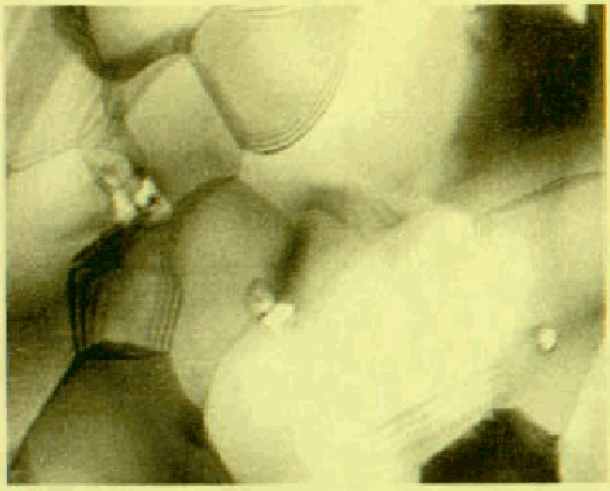

(a)

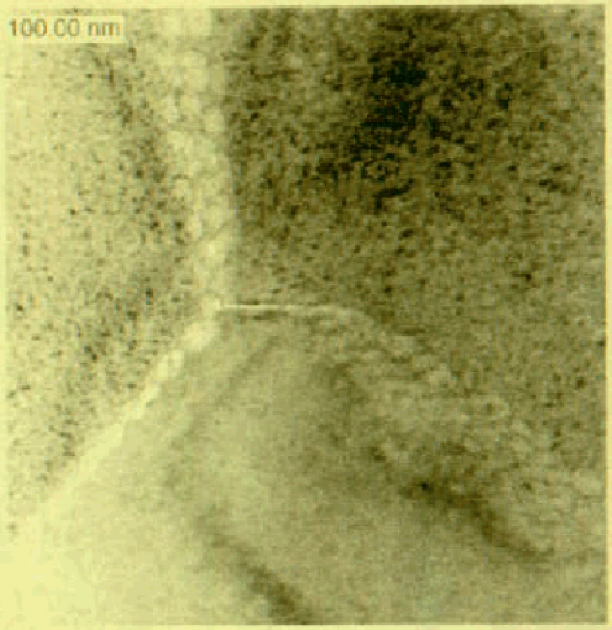

(b)

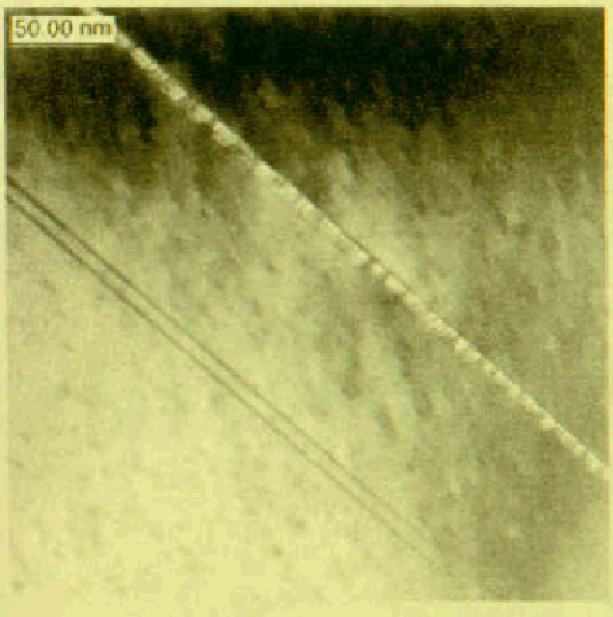

(c)

Fig. 6.

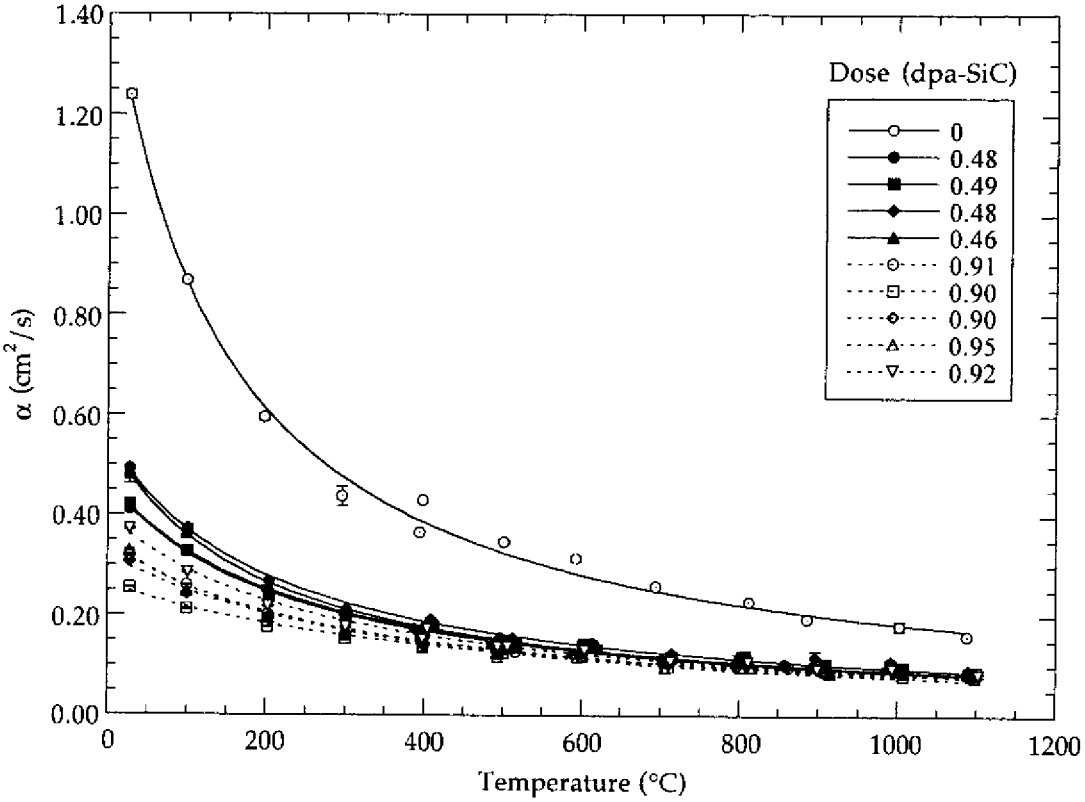
Dose (dpa-SiC)
0
0.48
0.49
0.48
0.46
0.91
0.90
0.90
0.95
0.92
α (cm²/s)
Temperature (°C)
1.40
1.20
1.00
0.80
0.60
0.40
0.20
0.00
0
200
400
600
800
1000
1200

Fig. 7.

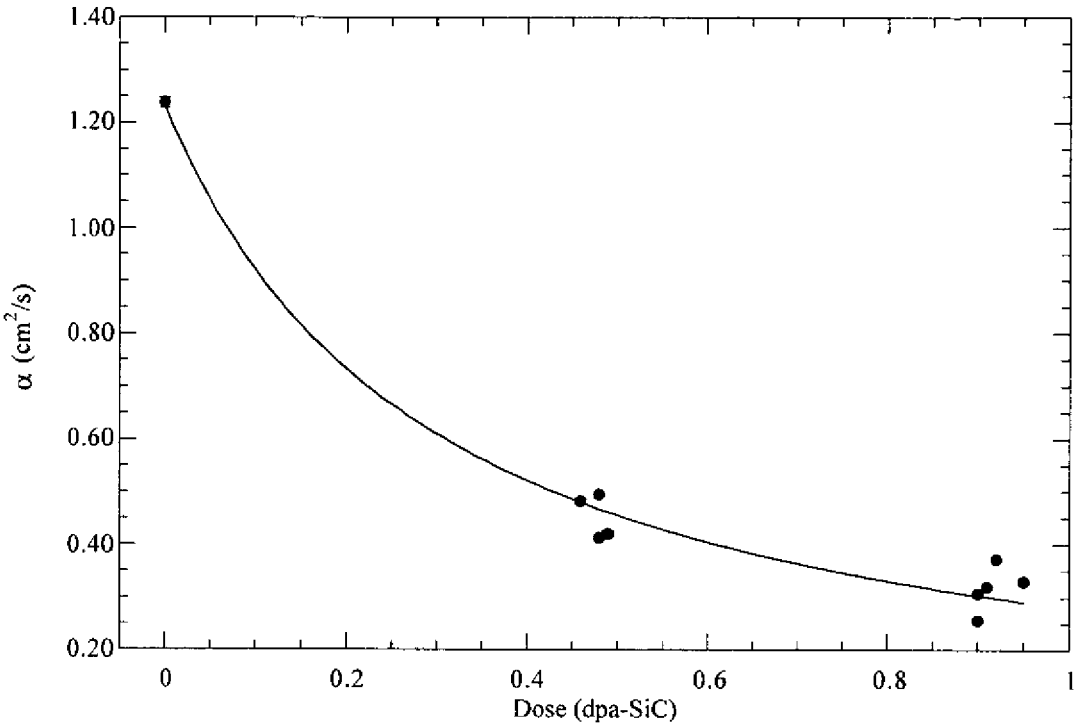

Fig. 8.

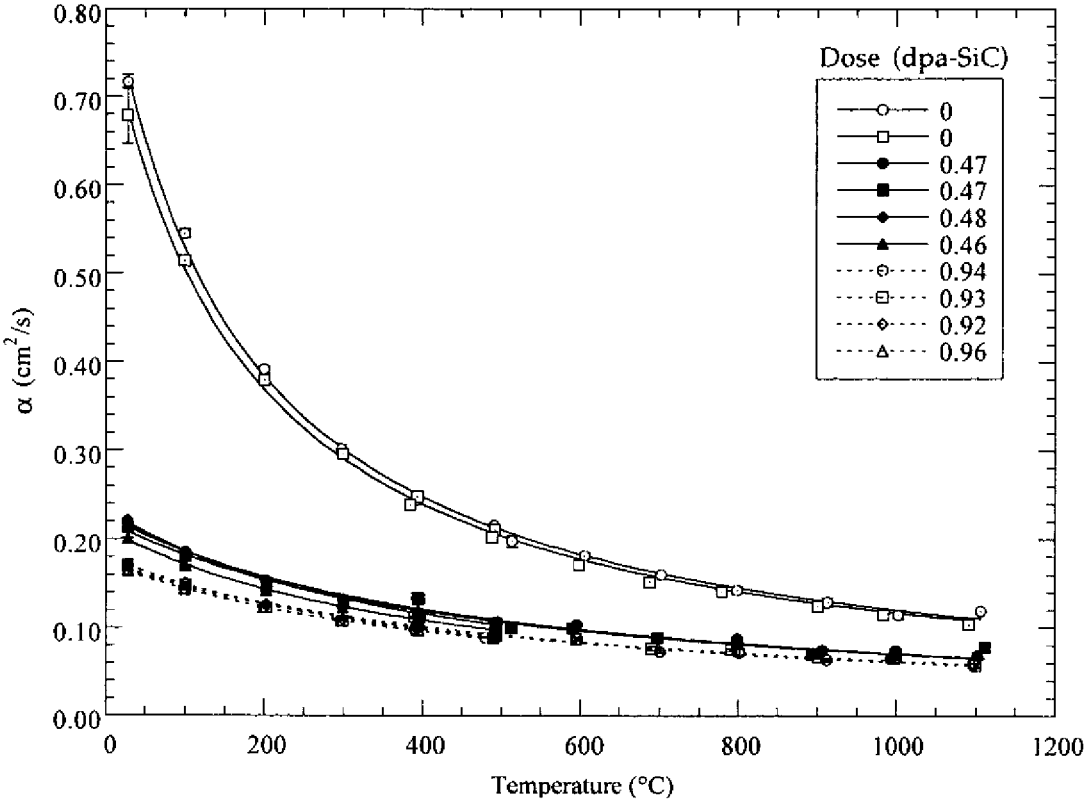
Dose (dpa-SiC)
0
0
0.47
0.47
0.48
0.46
0.94
0.93
0.92
0.96
α (cm²/s)
Temperature (°C)
0.00
0.10
0.20
0.30
0.40
0.50
0.60
0.70
0.80
0
200
400
600
800
1000
1200

Fig. 9.

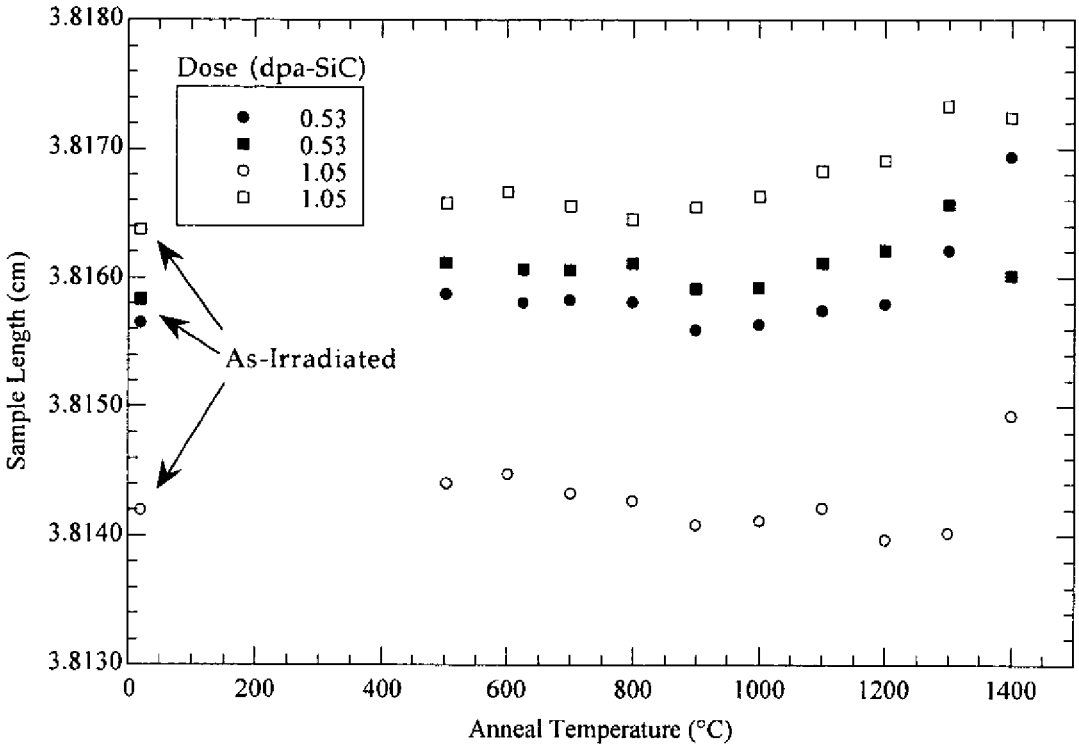
Dose (dpa-SiC)
0.53
0.53
1.05
1.05
As-Irradiated
Sample Length (cm)
3.8180
3.8170
3.8160
3.8150
3.8140
3.8130
0
200
400
600
800
1000
1200
1400
Anneal Temperature (°C)

Fig. 10.

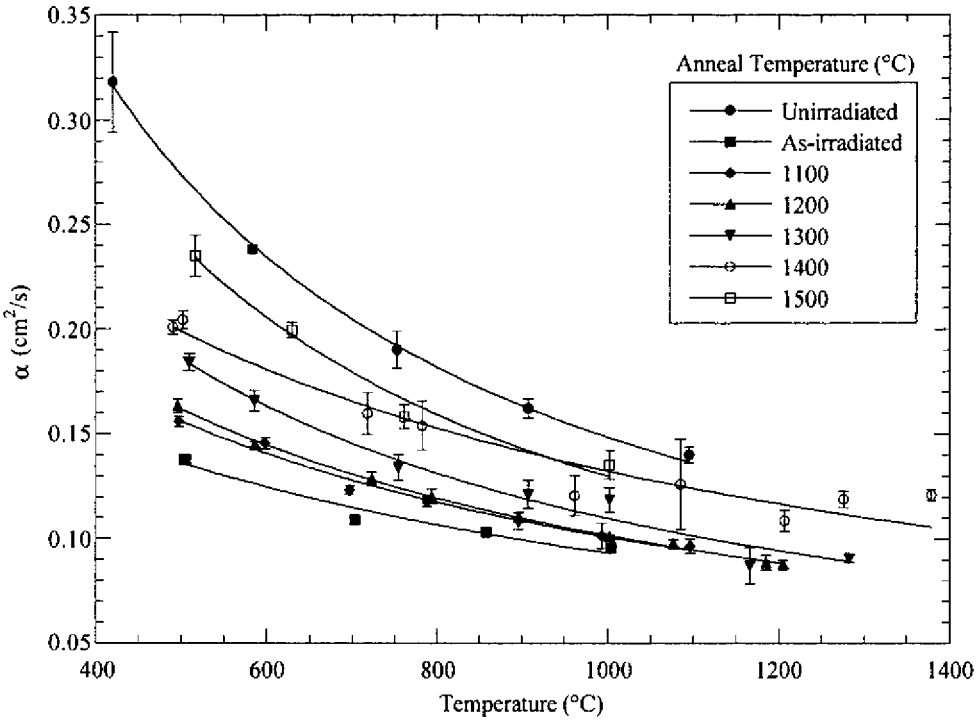
Anneal Temperature (°C)
Unirradiated
As-irradiated
1100
1200
1300
1400
1500
α (cm²/s)
Temperature (°C)
0.35
0.30
0.25
0.20
0.15
0.10
0.05
400
600
800
1000
1200
1400

(a)

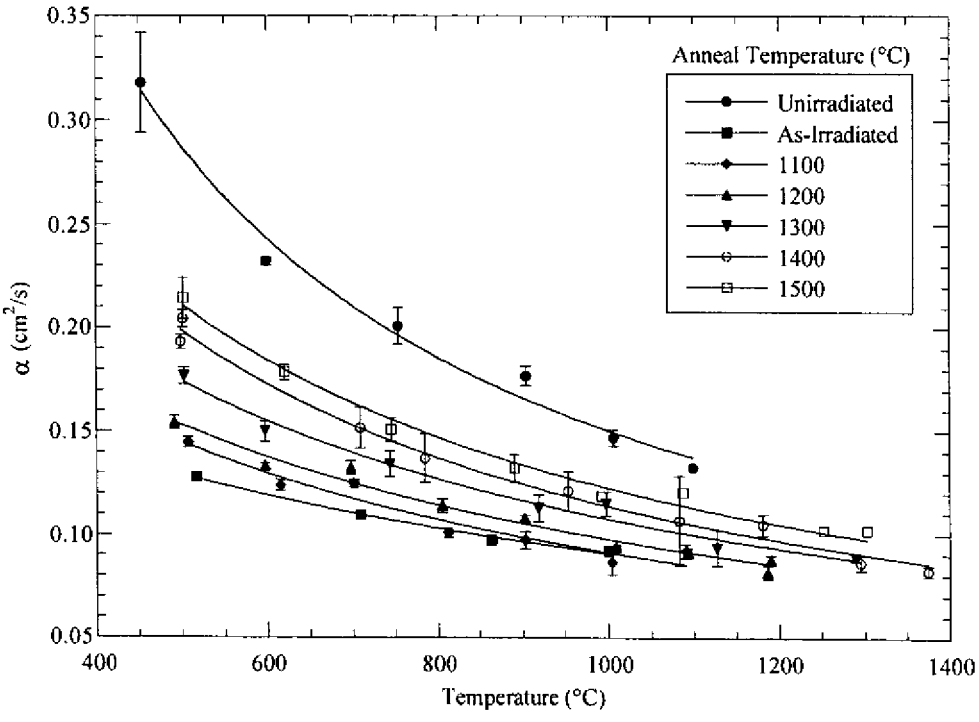
Anneal Temperature (°C)
Unirradiated
As-Irradiated
1100
1200
1300
1400
1500
α (cm²/s)
Temperature (°C)
0.35
0.30
0.25
0.20
0.15
0.10
0.05
400
600
800
1000
1200
1400

(b)

Fig. 11.

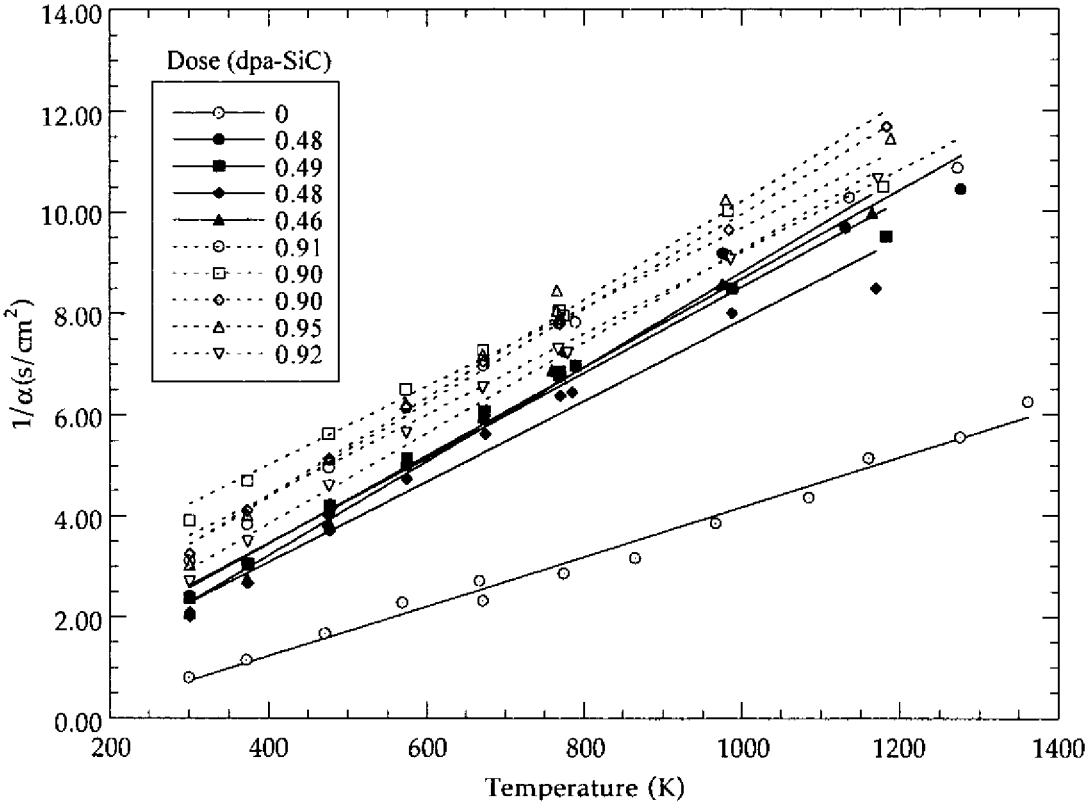
Dose (dpa-SiC)
0
0.48
0.49
0.48
0.46
0.91
0.90
0.90
0.95
0.92
1/α(s/cm²)
Temperature (K)
14.00
12.00
10.00
8.00
6.00
4.00
2.00
0.00
200
400
600
800
1000
1200
1400

Fig. 12.

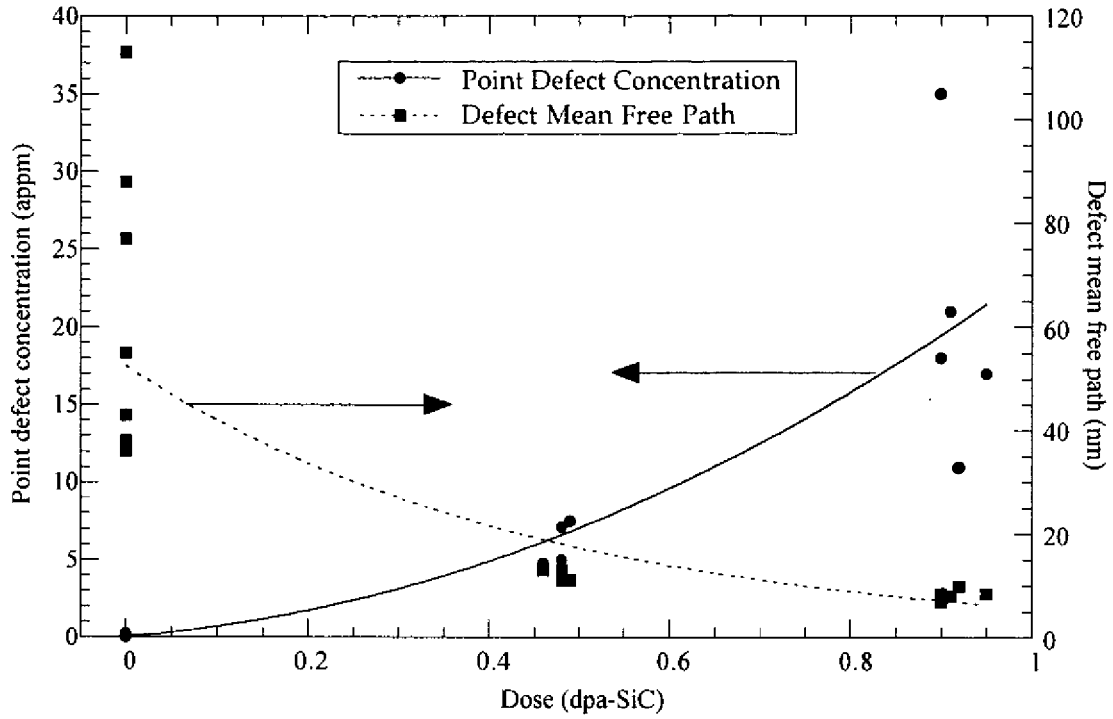
Point Defect Concentration
Defect Mean Free Path
Point defect concentration (appm)
Defect mean free path (nm)
Dose (dpa-SiC)
0
5
10
15
20
25
30
35
40
0
20
40
60
80
100
120
0
0.2
0.4
0.6
0.8
1

Fig. 13.

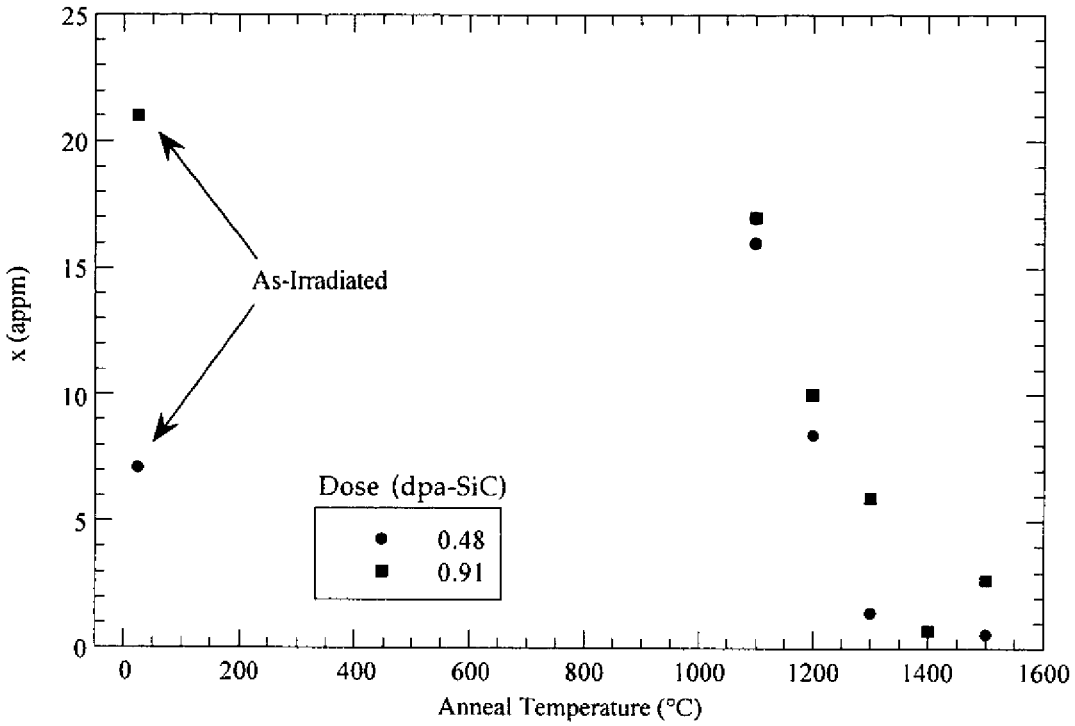
25
20
15
10
5
0
x (appm)
As-Irradiated
Dose (dpa-SiC)
0.48
0.91
0
200
400
600
800
1000
1200
1400
1600
Anneal Temperature (°C)

Fig. 14.

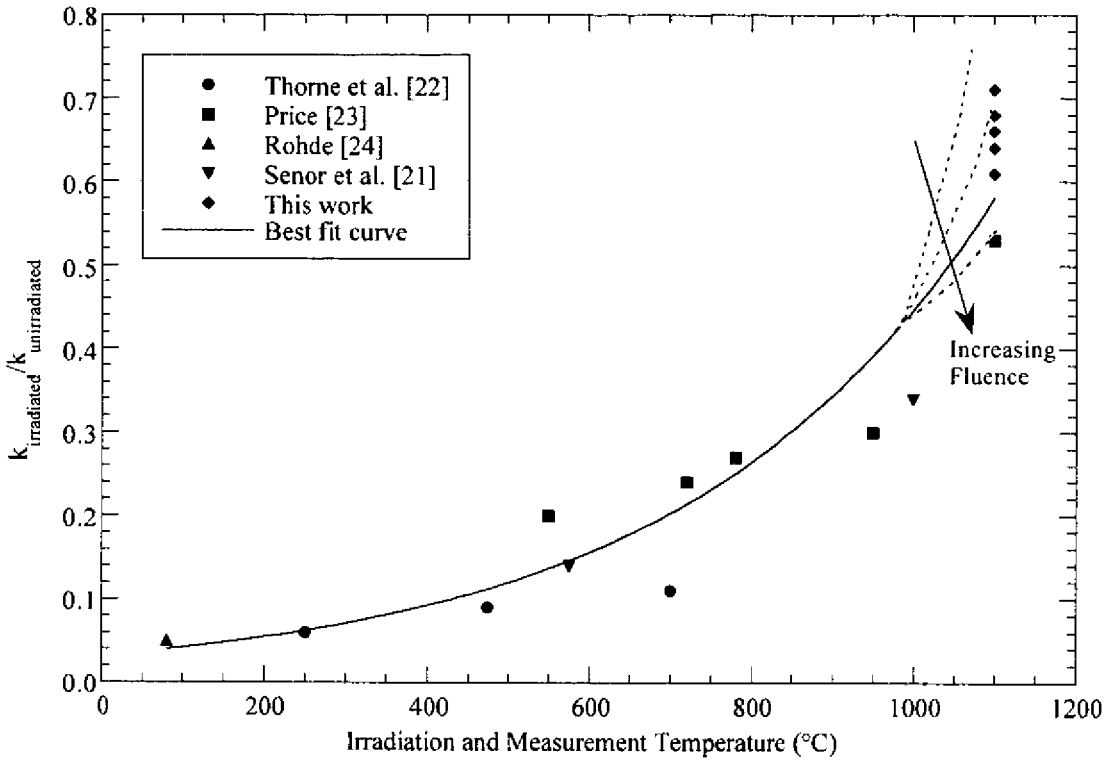
Thorne et al. [22]
Price [23]
Rohde [24]
Senor et al. [21]
This work
Best fit curve
Increasing Fluence
$k_{irradiated}/k_{unirradiated}$
Irradiation and Measurement Temperature (°C)
0.0
0.1
0.2
0.3
0.4
0.5
0.6
0.7
0.8
0
200
400
600
800
1000
1200

Table 1. Average Values for Irradiation-Induced Linear Swelling after Irradiation at Approximately 1100°C

Material	0.5 dpa-SiC (%)	1.0 dpa-SiC (%)
CVD SiC	0.0681 ± 0.0114	0.1201 ± 0.0200
Hexoloy SA	0.1140 ± 0.0055	0.1719 ± 0.0250

Table 2. Dislocation Loop Average Diameter and Areal Density Measured from the TEM Micrographs in Irradiated CVD SiC and Hexoloy SA

Material	Dose (dpa-SiC)	Post-Irradiation Anneal (°C/min)	TEM Images	Loop Avg Diameter (nm)	Loop Density (loops/nm^2)
CVD SiC	0.49	-	Fig. 2b	3.4	4.7×10^{-3}
CVD SiC	0.90	-	Fig. 2c	3.9	2.5×10^{-3}
CVD SiC	0.48	1500/60	Figs. 4a, 4b	4.2	1.4×10^{-3}
CVD SiC	0.91	1500/60	Fig. 4c	7.2	1.3×10^{-3}
Hexoloy SA	0.47	-	Fig. 5b	4.6	3.6×10^{-3}
Hexoloy SA	0.94	-	Fig. 5c	4.4	5.2×10^{-3}

Table 3. Calculated Pre- and Post-Irradiation Point Defect Concentrations for the CVD SiC Samples

Sample	Dose (dpa-SiC)	A (s/cm^2)	B (s/cm^2 - K)	R^2	l_d (nm)	x (appm)
ZZ/	0	-0.765	0.00527	0.995	38	0.18
D049	0	-0.732	0.00491	0.985	43	0.13
D040	0	-0.897	0.00593	0.998	36	0.23
D042	0	-1.334	0.00588	0.986	88	0.015
D044	0	-1.244	0.00621	0.983	55	0.062
D045	0	-1.740	0.00708	0.990	113	0.0072
D046	0	-1.451	0.00645	0.992	77	0.023
D040	0.48	-0.038	0.00872	0.984	11	7.1
D041	0.49	0.091	0.00842	0.987	11	7.5
D042	0.48	-0.089	0.00796	0.977	13	5.0
D043	0.46	-0.501	0.00931	0.992	13	4.8
D044	0.91	1.198	0.00803	0.980	7.9	21
D045	0.90	1.902	0.00778	0.981	6.7	35
D046	0.90	0.643	0.00933	0.998	8.4	18
D047	0.95	0.535	0.00968	0.985	8.4	17
D050	0.92	0.240	0.00902	0.995	9.9	11